



# AC losses of Roebel and CORC<sup>®</sup> cables at higher AC magnetic fields and ramp rates

M D Sumption<sup>1</sup> , J P Murphy<sup>2,3</sup>, T Haugan<sup>4</sup>, M Majoros<sup>1</sup>, D C van der Laan<sup>5</sup> , N Long<sup>6</sup> and E W Collings<sup>1</sup>

<sup>1</sup> CSMM, MSE, The Ohio State University, Columbus, OH 43210, United States of America

<sup>2</sup> University of Dayton Research Institute, Dayton, OH 45469-0073, United States of America

<sup>3</sup> Universal Energy Systems, Dayton, OH 45432, United States of America

<sup>4</sup> Aerospace Systems Directorate of the Air Force, Research Laboratory, Dayton, OH, Wright-Patterson AFB, 45433, United States of America

<sup>5</sup> Advanced Conductor Technologies and University of Colorado, Department of Physics, Boulder, CO, United States of America

<sup>6</sup> Robinson Research Institute, Victoria University of Wellington, Dayton, OH, New Zealand

E-mail: [sumption.3@osu.edu](mailto:sumption.3@osu.edu)

Received 17 August 2021, revised 9 November 2021

Accepted for publication 19 November 2021

Published 29 December 2021



## Abstract

We have measured ReBCO coated conductor-based conductor on round core (CORC<sup>®</sup>) and Roebel cables at 77 K in a spinning magnet calorimeter, which subjected the tapes in the samples to a radial magnetic field of 566 mT (peak) at frequencies up to 120 Hz (272 T s<sup>-1</sup>, cyclic average) with an approximately sinusoidal waveform. The samples were oriented such that the field applied to the tapes within the cables was entirely radial, simplifying subsequent analysis. An expression for loss which included hysteretic, flux creep and eddy current losses was fit to both the CORC<sup>®</sup> and the Roebel cables. This expression allowed easy comparison of the relative influence of eddy currents and flux creep (or power-law behavior) effects. The loss of both the CORC<sup>®</sup> and Roebel cables measured here were seen to be essentially the sum of the hysteretic loss, flux creep effects, and the normal metal eddy current losses of the individual tapes. The losses of these cables were measured at high  $B \times dB/dt$  with no coupling current loss observed under the present preparation conditions. The influence of flux creep effects on loss were not negligible. The losses of the CORC<sup>®</sup> cable per meter of tape were seen to be reduced from the case of a flat tape because of the helical geometry of the tapes.

Keywords: ac losses, ReBCO cables, CORC, Roebel

(Some figures may appear in color only in the online journal)

## 1. Introduction

Superconducting, coated conductor ReBCO strands and cables are of interest for a variety of applications, including medical imaging, particle beam steering, power transmission, and rotating machinery, among others. In the area of rotating machinery, we can include wind turbine generators as

well as motors and generators for propulsion and power, the latter in particular for aircraft applications [1]. For some of these applications there is a strong need to characterize and understand the AC losses of the ReBCO conductors at high frequency (from a few Hz to hundreds of Hz) and modest field (0.5 T to a few Tesla). Wind turbine generators, for example, operate in the few Hz range, while

some of the windings of motors or generators may experience hundreds of Hz. Of course, such systems may alternatively employ Bi-based superconductors,  $\text{MgB}_2$ , or other superconducting strand types, but ReBCO conductors have a number of compelling properties including high operating temperatures and high critical current ( $I_c$ ) performance, and so are of significant interest for these applications. Particular applications may use either individual tapes or cables of such tapes. Two well-known ReBCO cable types are conductor on round core (CORC<sup>®</sup>) [2, 3], and Roebel cables [4]. All of these conductors are known to have relatively high AC losses due to the width of the ReBCO tape, and thus there are a significant number of reports on their AC loss properties.

Most AC loss measurements on ReBCO strands or cables have been performed either at high frequencies at low applied magnetic field amplitudes [5–15] (typically 100–200 Hz and 100 mT), or higher fields (up to 8 T and even higher) but at low frequencies (typically mHz) [16, 17]. Loss measurements for CORC<sup>®</sup> [5–9] and Roebel cable [10–15] not only suffer these same limitations, but also require larger sample lengths than individual tapes. The high field amplitude but low frequency measurements are not easy to accurately project to the high frequency regime with confidence, and the lower amplitude but high frequency results are in some cases not very far away from full penetration fields for the conductors, which also makes less certain the projections of loss to the regimes of interest. Nevertheless, much interesting work on this topic has been generated, both experimental and computational. The recent work by Yagotintsev *et al* [17] is an excellent experimental study of losses of CORC and Roebel cables at 4.2 K and 77 K, with different surface preparations. Other work has included measurements on CORC-like conductors with few layers [18] or various layer designs [19]. The influence of Cu core contributions to the loss [8, 20] have been explored, and also the striations and filament-to-filament coupling within the strand of a striated CORC-like cable [7, 21, 22]. Numerous works on numerical modeling have been performed, a recent paper looks at the influence of twist on filamentary loss [23]. In a number of works, modeling and measurement are combined, see for example [24, 25]. AC loss for Roebel cables has also been quite active, with work on measurements and modeling [4, 10, 16, 17, 26, 27].

While much work has been done on the loss of such cables, this manuscript contains important new results on the AC loss of High Temperature Superconducting (HTS) cables at somewhat more difficult to reach regimes, using a measurement system capable of magnetic field ramping rates of up to  $272 \text{ T s}^{-1}$  with field amplitudes of more than 566 mT. These results combine high ramping rates with larger  $B_{\text{max}}$  values on cables and are relevant to high impact HTS applications in superconducting motors and generators. To do this, we use a recently described spinning magnet calorimeter (SMC) [28]. This test device has a spinning rotor that consists of a set of permanent magnets arranged in a Halbach array, with the sample exposed to a rotating AC field of 566 mT (peak) and a resulting  $\text{dB}/\text{dt}$  of  $272 \text{ T s}^{-1}$  for the radial component (tangential component

$B_{\text{max}} = 242 \text{ mT}$ ,  $\text{dB}/\text{dt} = 125 \text{ T s}^{-1}$ ). This corresponds to a frequency of 120 Hz for our machine. Two ReBCO cable types were measured for this work, a CORC<sup>®</sup> cable and a Roebel cable. For the CORC<sup>®</sup> cable, a straight segment of the tape used in the cable was available, and was thus measured for comparison. Below we first discuss sample and measurement details before moving on to our analysis methods and measurement results. We then compare CORC<sup>®</sup> cable loss with that of the tape from which it was wound, as well as provide measurements on Roebel cable under the same measurement conditions. The CORC<sup>®</sup> and Roebel cable results are not directly compared because the ReBCO conductor used to assemble them was different. Nevertheless, we do see that the results here show the lack of coupling current contributions even at very high field ramp rates for both CORC<sup>®</sup> and Roebel cables in their as-received states. Loss measurements are compared to loss models, and it is shown that the loss in the cables is due to hysteretic and eddy current losses alone, as well as a flux creep modification to the hysteretic loss.

## 2. Experimental

### 2.1. Samples

In this work, two different HTS cables assembled with coated conductors were measured for AC loss in a time varying magnetic field applied perpendicular to the cable length (table 1). The first cable was a segment of a two-layer CORC<sup>®</sup> superconducting cable from Advanced Conductor Technologies LLC. The cable had an outer diameter (OD) of 5 mm and a former made from 304 stainless steel (4.7 mm OD, 3.13 mm inner diameter (ID)) [5]. The coated conductor REBCO tape, manufactured by Superpower, was 4 mm wide and 0.09 mm thick with a nominal self-field  $I_c$  of 100 A at 77 K. The cable had two layers, each with three tapes, leading to a nominal cable  $I_c$  of 600 A (77 K, self-field) with a 0.1 mm gap between the tapes [5]. The twist pitch of the cable,  $L_p = 20 \text{ mm}$ , with the outer layer twisted in an opposite sense to the inner layer. The length of a helical winding as compared to the length along the direction of the helix is  $[1 + (\pi D/L_p)^2]^{1/2}$ . Given the  $L_p$  and  $D$  of the present cable, this factor is 1.28, and with six tapes in the cable, each meter of cable has 7.68 m of strand. The sample in this case was 8 cm long, leading to 0.614 m of strand.

Also measured in this work was a Roebel cable from Robinson Research Institute. This cable [12] was 10 cm long, 12 mm wide, 1.5 mm thick, and had a pitch length of 300 mm and a self-field  $I_c = 1537 \text{ A}$  (77 K, measured). It was assembled from 15 strands. These strands were cut from a 12 mm wide starting tape. The final strands had a slight zig-zag pattern as is common for the strands of HTS Roebel cables. The final strand width (width of the straight portion) was 5 mm. These two cables are assembled from different REBCO tapes, and thus are not directly comparable to one another without adjusting for the relative  $I_c$  values. Here we present the results in parallel, but do not attempt to compare them directly on a per ampere basis.

**Table 1.** Cable specifications.

Cable	OD/w × t (mm)	L <sub>p</sub> (mm)	No. tapes	I <sub>c</sub> (A) (77 K, SF)	Tape width (mm)	Sample L (cm)
CORC	5.0	20	6 (2 × 3)	600	2	8.0
Roebel	12 × 1.5	300	15	1537	5	10.0

## 2.2. Measurements

The two cables described above were measured in a recently described SMC [28]. This test device has a spinning rotor which consists of a set of permanent magnets arranged in a Halbach array, with the sample exposed to a rotating AC field of 566 mT (peak) and a resulting  $dB/dt$  of  $272 \text{ T s}^{-1}$  for the radial component (tangential component  $B_{\text{max}} = 242 \text{ mT}$ ,  $dB/dt = 125 \text{ T s}^{-1}$ ). A 3D schematic view of the SMC is shown in figure 1(a), where a cut-away shows the spinning rotor with the magnet array, and spaces for samples at the periphery (located roughly where a ‘stator’ might be if this was, e.g. a generator). Two potential types of inserts are shown above the device, the one on the right shows our present situation. In this configuration, the light green region is the outer LN<sub>2</sub> bath for a calorimeter, which in practice remains fixed in the SMC, but is shown here to be extracted for the purposes of explanation. Inside of this is shown the inner calorimeter (dark green), with a sample placed within. This sample is immersed in LN<sub>2</sub>, with the gas flow from boil-off from this inner calorimeter used for AC loss measurement, further details are given in [28]. Samples measured in the SMC are placed a small radial distance from a spinning rotor containing magnets with pole orientations that alternate along the circumference (figure 1(b)). The sample space experiences radial and tangential fields that are approximately sinusoidal in character, with the details of the waveform shape and harmonics given in [28]. Note that here and elsewhere we refer to an average  $dB/dt$  obtained by taking the total field sweep and dividing by the total time of the cycle. Thus, even though there is a momentary peak value of  $426 \text{ T s}^{-1}$ , the instantaneous  $dB/dt$  varies throughout the cycle because of the sinusoidal nature of the waveform, and the average or effective value is maybe more useful to quote.

For all the measurements in this work the tapes and cables were oriented in a plane horizontal to the rotational axis of the SMC, as shown in figure 1(b). The samples were placed with their length along the tangential field direction, which leads to a situation where tangential fields are only present within the local plane of the coated conductor tapes that are assembled to form the CORC<sup>®</sup> and Roebel cable, and radial fields are the only ones that can become perpendicular to the coated conductor tape within these cables. This is also the case for the single tape that was measured. Thus, tangential fields were only applied to the thin dimensions of the REBCO tapes for all samples, both tapes and cables, making direct tangential loss contributions negligible in all cases. Of course, the presence of a tangential field can modify  $\Delta M$  vs  $B_{\text{radial}}$  because while a  $B_{\text{tangential}}$  which is only within the conductor plane does not directly generate appreciable screening currents, it can contribute

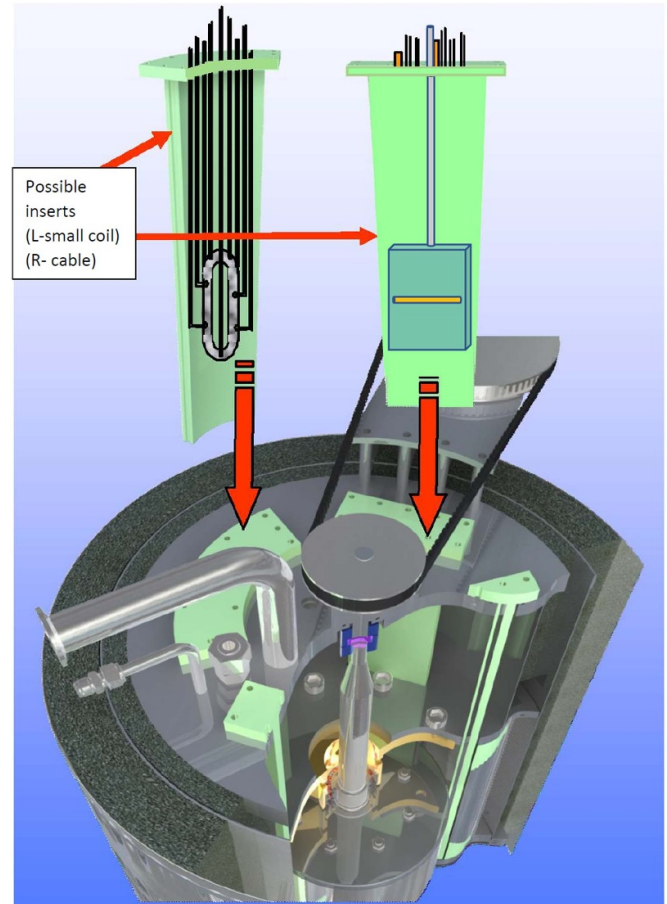


**Figure 1(a).** 3D schematic of spinning magnet calorimeter system with cut away view, and calorimeter with sample inserts. On left is shown an opening into which a small coil can be measured, on the right we show our present configuration, which includes the outer nitrogen bath (shown in light green), the inner calorimeter shown in darker green, and the sample placement (sample shown as yellow rod, positioned in a horizontal plane).

to the total  $B$  which the conductor experiences, thereby reducing somewhat the  $J_c$  via its dependence on total  $B$ . We can estimate the influence of the small deviation from sinusoidal behavior (for this radial component) by summing the square of the frequency weighting by its amplitude to compare to a full weighted 30 Hz value. The difference in terms of eddy current loss being less than 5% (and zero for hysteretic loss) is ignored [28]. Thus, in the present sample orientation, with samples placed horizontally, the tapes in the sample experience only the radial field of the system, and we can treat the applied field as a simple sinusoidal of amplitude 566 mT. Sample AC loss

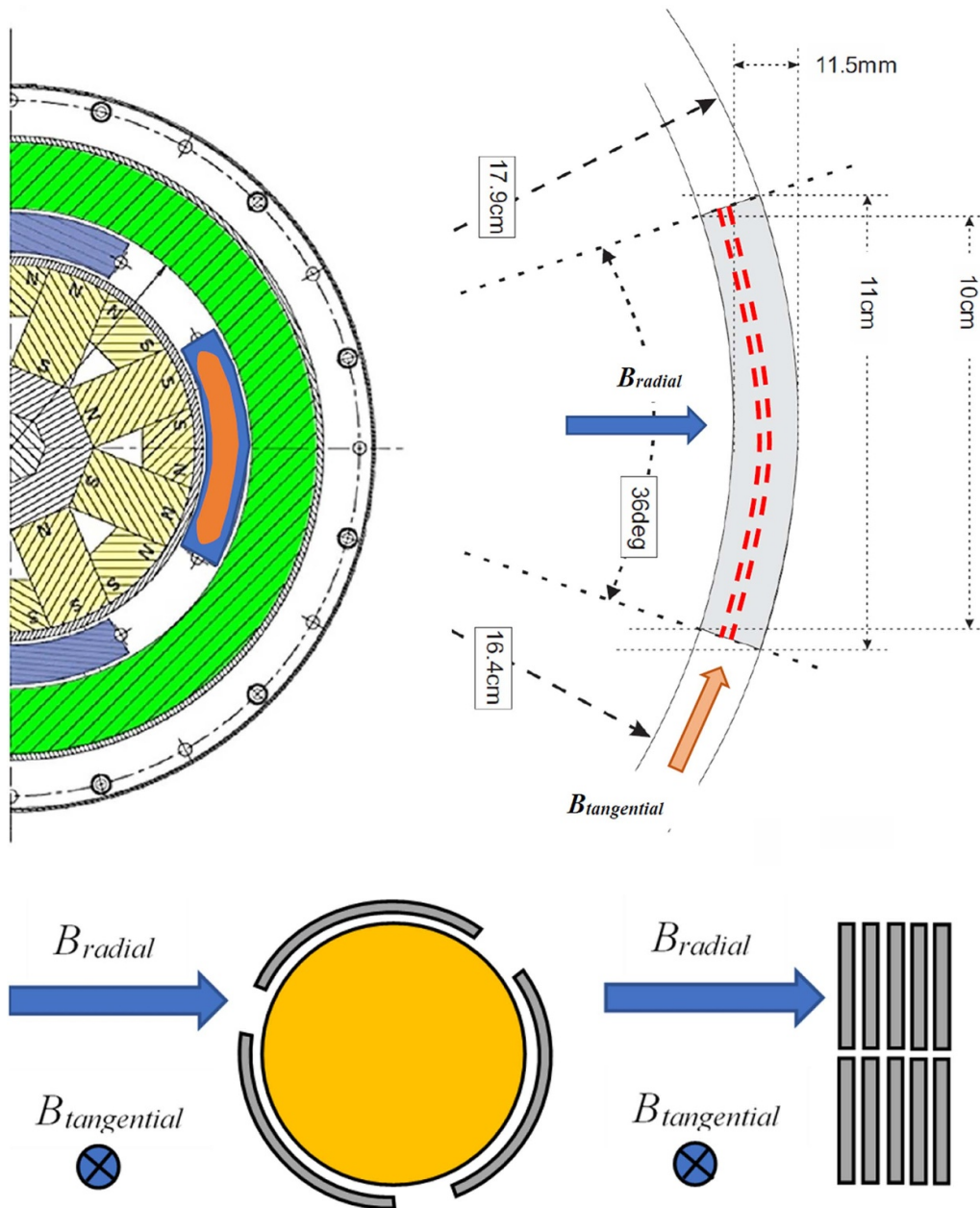


**Figure 1(b).** Orientation of samples in the SMC. System rotational axis is vertical; view is looking down from above. Left shows the SMC rotor magnet geometry (half of the system shown, yellow and gray), solid blue rectangle shows the LN<sub>2</sub> bath (outer bath, used for heat interception), and orange arc shows the sample holder/inner calorimeter. On the right is shown the inner calorimeter (in gray, note: actual edges of the calorimeter are rounded, as shown at left). Also shown at right is the sample placement. All samples were arranged in the horizontal plane of the SMC. All samples were flexible and were affixed parallel to the tangential direction. The red dashed lines show an ‘envelope’ where samples can be placed for this horizontal sample arrangement. Below are shown the radial and tangential fields relative to schematic representations of the CORC<sup>®</sup> (left) and Roebel (right) cable samples. It can be seen that the tangential fields are only present in the local plane of the coated conductor tapes within the cables, and radial fields are the only ones which can become perpendicular to the coated conductor tapes in the cables. The case for the single tape is similar to that of the Roebel cable.

is measured using nitrogen boiloff from a double wall calorimeter feeding a gas flow meter. The system is calibrated using the power input from a known resistor, as discussed in [28], and background losses are removed (this can lead to a small data scatter even at zero excitation). For comparison to the CORC<sup>®</sup> cable, a straight segment of the tape used in the cable was also measured in a field perpendicular to the wide face of the tape.

### 2.3. Analysis

Before we present the measurement results, it is useful to show the treatment we will use to perform the loss analysis. In the case of field applied perpendicular to the wide face of a coated conductor tape, the hysteretic loss can be written, using a critical state model (CSM), as [29–34]

$$P_{\text{hys,v,cs}} = N(B_{\text{max}})wJ_c B_{\text{max}}f \quad (1)$$

where  $P_{\text{hys,v,cs}}$  is the critical state hysteresis power per unit volume in Watts,  $w$  is the tape width,  $f$  is the frequency,  $B_{\text{max}}$  is the field amplitude, and  $N(B_{\text{max}})$  is a prefactor that tends to unity for applied fields above the penetration field [29–34]. The normal metal eddy current loss per unit volume for a flat tape (from Muller [31], equation (16)) modified to a convenient form is

$$P_{\text{ed,v}} = \frac{\pi^2}{6\rho} [B_{\text{max}}wf]^2 \quad (2)$$

where  $\rho$  is the resistivity of the Cu. This expression is valid as long as we are below the skin depth frequency, given [34] as

$$f_s \cong \frac{1}{2\pi} \frac{\rho}{\mu_0 x^2} \quad (3)$$

where  $x$  is the metal thickness in question. A simple calculation shows that for both the Cu stabilizer and the stainless 304 core, the critical frequencies are much greater than we are using in these experiments. Equations (1) and (2) can be combined and put in the form of power loss per unit length as

$$P_{\text{tot,L,cs}} = wI_c B_{\text{max}}f + \frac{\pi^2}{6\rho} [B_{\text{max}}wf]^2 wt \quad (4)$$

where  $P_{\text{tot,L,cs}}$  is the total loss of the tape per unit length in the CSM,  $t$  is the thickness of Cu in the whole tape, and setting  $N = 1$ . In both equations (1) and (4) we have assumed a CSM, and in fact a  $B$  field independent  $J_c$ . Of course, this latter assumption can be relaxed, and a field dependence can be included at the cost of additional complexity. In principle, we should also account for the eddy current loss in the stainless steel core for the CORC<sup>®</sup> wire, which can be found using a similar expression to that of equation (2), with the factor of six replaced by a factor of four based on geometry considerations. However, as discussed below in the results section, the losses in the stainless steel core are sufficiently small that core losses can be ignored for this cable.

We should also consider the effect of flux creep on loss [35, 36]. One way to estimate this is the approach of Pust *et al* [37]. A second way to do this is to use a power law model (PLM) rather than a CSM. For a PLM [38–40],

$$E = E_c \left( \frac{I}{I_c} \right)^n \quad \text{thus} \quad \left( \frac{E}{E_c} \right)^{1/n} = J/J_c$$

and then  $J = J_c \left( \frac{E}{E_c} \right)^{1/n}$ . (5)

During a transport  $I$ – $V$  measurement,  $J$  is the current density that flows when an electric field of magnitude  $E$  is applied, and  $J_c$  is the current density that flows under an electric field of  $E_c$  (typically either  $1.0 \mu\text{V cm}^{-1}$  or  $0.1 \mu\text{V cm}^{-1}$ ), which also correlates in a time changing field (e.g. in an AC loss measurements) as  $E \propto (dB/dt)$ . For the CSM model,  $J_c$  is uniquely defined (equivalent to letting  $n \rightarrow \infty$  in equation (5)), and thus a unique (i.e. frequency independent) hysteretic loss can also

be defined, as in equation (1). We note that in the absence of extrinsic defects  $n \cong U_0/k_b T$  ([40], see equation (8)), providing the explicit connection to flux creep, where, phenomenologically,  $M(t) = M_0[1 - (k_b T/U_0)\ln(t/t_0)]$ . To calculate the loss associated with the superconductor alone in the power law case, we replace  $J_c$  with  $J = J_c(E/E_c)^{1/n}$  in equation (1), leading to a magnetization loss in a power law superconductor,  $P_{\text{hys,v,pl}}$ , of

$$P_{\text{hys,v,pl}} = wJB_{\text{max}}f = wB_{\text{max}}fJ_c \left( \frac{E}{E_c} \right)^{1/n}$$

$$= wB_{\text{max}}fJ_c \left[ \frac{(dB/dt)}{(dB/dt)_c} \right]^{1/n}. \quad (6)$$

Since  $E = (w/2)(dB/dt)$ , and using an average  $dB/dt$  defined as  $dB/dt = 2\pi B_m f$ , then

$$P_{\text{hys,v,pl}} \cong wJ_c B_{\text{max}}f \left( \frac{f}{f_c} \right)^{1/n}. \quad (7)$$

Here we note that unlike the CSM hysteretic loss,  $P_{\text{hys,v,pl}}$  is a function of frequency. Equation (7) is a simple and approximate approach, but agrees with the result from Thakur in the limit of  $B_m \gg B_p$  (see [38], equation (17)). If we now compare equation (7) to equation (1), we see that they agree at  $f = f_c$ . But, as evident from equation (6), the  $(dB/dt)_c$  and  $f_c$  required for this agreement are such that the electric field is that of the criterion at which  $J_c$  is defined, namely  $E_c$ . Then  $E = E_c \cong (w/2)(dB/dt)_c = \pi w B_{\text{max}}f$ , such that  $f_c \cong (E_c)/\pi w B_{\text{max}}$ . At  $f_c$ , the superconductor-only power loss for the CSM and the PLMs agree most closely. A similar approach to defining  $f_c$  was taken by Brandt [39] and Grilli *et al* [35], see also [41], but they chose an  $f_c$  with the aim of maximizing the susceptibility, and thus chose the penetration field rather than  $B_{\text{max}}$  in the definition of  $f_c$ . As shown by Grilli this choice leads to reasonable agreement in terms of critical state and power law susceptibility for  $B_{\text{max}} > B_p$ . But here we use an  $f_c$  based on  $B_{\text{max}}$ , as it gives a better match for our conditions, and is more practical to apply for our experiment.

In this case the total loss for the tape is given by

$$P_{\text{tot,L,pl}} \cong wI_c B_{\text{max}}f \left( \frac{f}{f_c} \right)^{1/n} + \frac{\pi^2}{6\rho} [B_{\text{max}}wf]^2 wt \quad (8)$$

and the influence of both eddy currents and creep are now included in the loss expression. These approximate expressions assume that  $B_{\text{max}} > B_p$ , and that  $J_c$  is independent of  $B$ . The formulation for superconductor loss (the first term) here follows from that of [35, 36, 38], although here we take the limit of  $B_{\text{max}} > B_p$ . At  $f = f_c$ , the losses of the critical state and power laws are similar, for  $f < f_c$ , equation (8) will give a lower loss than the CSM, for  $f > f_c$ , equation (8) will give a higher loss. We can re-write equation (8) as follows

$$P_{\text{tot,L,pl}} \cong wI_c B_{\text{max}}f + wI_c B_{\text{max}}f \left[ \left( \frac{f}{f_c} \right)^{1/n} - 1 \right] + \frac{\pi^2}{6\rho} [B_{\text{max}}wf]^2 wt. \quad (9)$$

In order to cast the power law modifications as an additive term for  $f > f_c$  (or subtractive term if  $f < f_c$ ). For the present experiment, assuming we use an  $I_c$  defined by  $E_c = 1 \mu\text{V cm}^{-1}$ , and for a 4 mm wide tape,  $f_c = (E_c)/\pi w B_{\text{max}} = 10^{-4} \text{ V m}^{-1}/(\pi \times 0.004 \text{ m} \times 0.566 \text{ T}) = 14 \text{ mHz}$ . Thus for this work,  $f > f_c$  and the second term of equation (9) is positive, i.e. the power law loss is greater than that of the CSM for all measurements presented in this work. It is interesting to estimate the field ramp rate that would correlate with this  $f_c$  for a typical Physical Properties Measurement System (PPMS) (or Vibrating Sample Magnetometer (VSM)) measurement. Assuming the same  $B_{\text{max}}$  but a triangular  $B$  vs  $t$  waveform more typical of such systems,  $\text{dB}/\text{dt} = 4B_{\text{max}}f = 32 \text{ mT s}^{-1}$ . Typical ramp rates achievable in PPMS systems are usually below  $15 \text{ mT s}^{-1}$ , so for such systems, the second term in equation (9) would typically be negative, and the power law conductor loss would be less than that estimated from the CSM. The above discussion is consistent with the well-known need to compare the electric field criterion between transport and magnetic measurements of  $J_c$ . We note that the effects of the flux creep term can be substantial. If we are measuring in a range of, for example  $10\text{--}100 \text{ mT s}^{-1}$ , and assign  $f_c = 14 \text{ mHz}$ , then at  $100 \text{ Hz}$ , the power law hysteretic loss will be larger than the critical state hysteretic loss (that at  $14 \text{ mHz}$  by a factor of  $(7142)^{1/35} = 1.26$ , or 26% if  $n = 35$ ,  $(7142)^{1/20} = 1.56 = 56\%$  if  $n = 20$ ).

Finally, we note that the above equations (8) and (9) are the loss of a ReBCO tape in a perpendicular applied field. It should apply to a good approximation to the Roebel cable in a perpendicular field if we use the final strand width of 5 mm. For the CORC<sup>®</sup> cable, the strands are helically wound. A simple calculation that estimates the average magnitude of the field perpendicular to the tape along a cycle of its twist [34] suggests that the loss of the helical tape should be lower by a factor  $2/\pi$  than the loss of a straight, untwisted tape in a perpendicular applied field. We note that the factor of  $2/\pi$  was intended to be applied to the hysteretic loss component of the tape. However, the same field magnitude variations apply for any eddy current components, but eddy current power loss goes as  $\text{dB}/\text{dt}$  squared, and so we should apply a factor of  $(2/\pi)^2$  on that basis. This leads to an expression for the loss of CORC cables of

$$P_{\text{tot,L,pl}} \cong \left(\frac{2}{\pi}\right) w I_c B_{\text{max}} f + w I_c B_{\text{max}} f \left[ \left(\frac{f}{f_c}\right)^{1/n} - 1 \right] + \frac{4}{6\rho} [B_{\text{max}} w f]^2 w t. \quad (10)$$

We can also estimate the penetration field for both cables, so that we can compare to our applied field sweep amplitude. For an isolated tape, the penetration field is given [34] by  $B_p = (\mu_0 I_c / \pi w) [1 + \ln(w/t)] \approx 93 \text{ mT}$  using the self-field  $I_c$  value of  $100 \text{ A}$  at  $77 \text{ K}$  [5]. For a CORC<sup>®</sup> sample, the tape is helically twisted around a core. Considered as an individual tape, some portions of the tape will become penetrated at fields determined by the field parallel expression for a tape, namely  $B_p = \mu_0 I_c / w \cong 30 \text{ mT}$ . However, other portions will not be fully penetrated until the  $B_p$  for perpendicular fields for tapes, the  $93 \text{ mT}$  noted above. For our purposes, we can

take the full penetration field of such a helical conductor to be  $93 \text{ mT}$ , since above this field sweep the loss would be linear with applied field sweep increases. For a many-layer conductor with tight windings, we could expect this to increase, ultimately approaching the case of the thick wall cylinder. Our cable is only two layers thick, so at an applied field of  $566 \text{ mT}$  we are well above  $B_p$  for the cable in any case.

In the case of the Roebel cable, we can compare the value for an isolated tape, again  $93 \text{ mT}$  (using the nominal  $I_c$  per tape of  $100 \text{ A}$  [12], and with  $J_{c,\text{eff}} = 15I_c/(wt)$ ) with that of a diluted superconductor [42] in conjunction with the expression for the penetration field of a rectangular bar [43], then we find  $B_p = (\mu_0 J_{c,\text{eff}} t / (2\pi)) [(2wt) \arctan(t/w) + \ln(1 + (wt)^2)] \approx 120 \text{ mT}$ . Again, we are well above either value with our applied field of  $566 \text{ mT}$ .

## 2.4. Results

Figure 2 shows the loss of the tape (per meter) used to make the cable. The sample was measured horizontally, perpendicular to the radial field direction in the SMC. We note that a flat tape gives the same result when mounted horizontally as it would if oriented vertically (a fact that was experimentally verified) because (a) the field is fully penetrated by the radial field in the sample over an angular distance much larger than the sample width, making the response to radial fields the same, and (b) the thin sample has a negligible response to the tangential fields applied perpendicular to the tape's thickness. As described in [28], because of the field dependence of the  $J_c$  of the tape (ranging from  $100 \text{ A}$  at self-field to  $\approx 20 \text{ A}$  at  $0.5 \text{ T}$ ) the  $I_c$  of the tape  $\approx 38 \text{ A}$  for field sweep values that range up to  $566 \text{ mT}$  (data of this tape is from [28]).

The linear curve (red dashed line) in figure 2 shows the calculated hysteretic loss of the tape for  $I_c = 35 \text{ A}$  (the first term of equation (9)), and the dashed blue line the flux flow or power law modification (the second term) where we have assumed  $n = 35$ . The green dashed line gives the eddy current contribution of the stabilizer where  $\text{RR} (77 \text{ K}) = 3.8$  (and a Cu thickness of  $40 \mu\text{m}$  top and bottom on the tape) [28]. Here, RR refers to the resistivity ratio of a material at ice point ( $0^\circ \text{C}$ ) as compared to its value at some lower temperature, here taken as  $77 \text{ K}$  (residual resistivity ratio) is RR when the lower temperature is absolute zero. RR values for Cu can vary, with higher numbers (up to 5.5 at  $77 \text{ K}$  for low defect, high purity Cu) to lower values for Cu which is less pure or has defects. Electroplated Cu has many defects associated with the plating process itself, and a RR value of 3.5–4 is not uncommon [44]. The  $\text{RR} (77 \text{ K}) = 3.8$  gives a Cu resistivity at  $77 \text{ K}$  of  $0.46 \mu\Omega \text{ cm}$ . We also must consider the eddy current losses in the stainless steel core. However, the resistivity of the stainless steel 304 used in the core is  $72 \mu\Omega \text{ cm}$ , such that relative to the Cu stabilizer there is a loss suppression of the stainless steel (SS) term (per unit volume) of 164 due to the much higher resistivity of the SS. A second loss suppression (relative to the eddy current loss in the superconducting tape stabilizer) occurs because the SS core is  $3.16 \text{ mm}$  wide, while the tape is  $4 \text{ mm}$  wide, and thus there is a further suppression factor of 1.6. There is a loss enhancement ratio per unit length of conductor of the ratio of

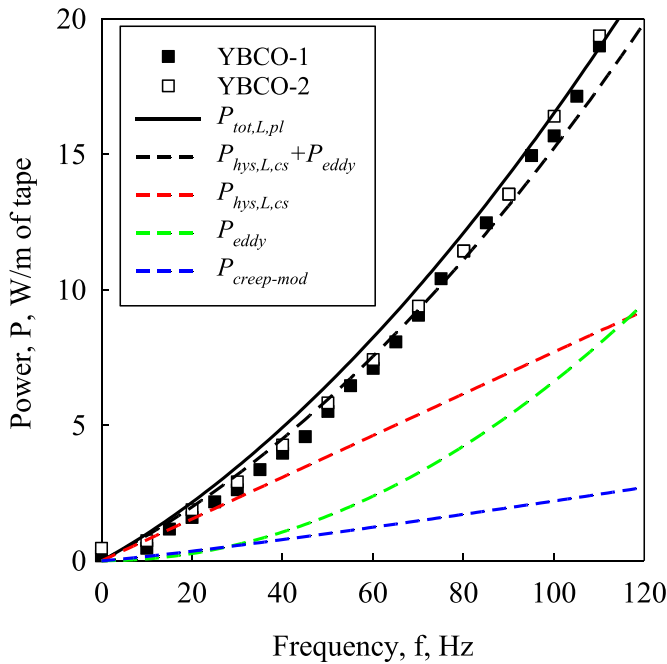


**Figure 2.** Loss for a flat, straight segment of tape (conductor used for CORC<sup>®</sup>). The black line is the calculation for a ReBCO tape with  $I_c = 35$  A, and including hysteretic loss (critical state), flux creep modification ( $n = 35$ ), and an eddy current loss component for a Cu strip  $80 \mu\text{m}$  thick with a  $RR = 3.8$  at  $77$  K [4]. Dashed red line is hysteretic component, blue line is flux creep modification, green is eddy current. Black dashed line is eddy current and hysteretic loss (without flux creep modifications) only.

the volumes (of the core vs the total stabilizer in a given cross section), which, per unit length causes an enhancement of 24. Overall, this leads to a factor of 11 times lower eddy current loss in the stainless steel core than in the stabilizer. This is sufficiently small to be ignored further in this work, but certainly could not be ignored if the core was itself Cu. The dashed black line gives the response of the hysteretic and eddy current contributions only, and the solid black line the summation of all loss terms. The agreement with the experimental data is reasonable.

Figure 3 shows the CORC<sup>®</sup> cable result (=cable loss (W)/total length of REBCO tape within sample (m)). For the tape sample of figure 2, mounting the sample vertically or horizontally would make no difference, as long as the tape was perpendicular to the radial field. Conversely, a round cable would have a non-negligible width exposed to transverse fields if the cable was measured with vertical orientation, but since we align the tape horizontally, we avoid such tangential field exposure, simplifying our analysis. In this case, *the tapes within the cable* only experience a radial field, approximately sinusoidal with time, of amplitude  $566$  mT.

We also plot the tape data of figure 2 along with the CORC<sup>®</sup> cable result in figure 3, and we see that the CORC<sup>®</sup> cable loss is lower than that of the tape it is wound with, on a per total tape length normalization basis. We can then apply the correction factors discussed in the analysis section to the calculated tape loss, as embodied in equation (10). This gives the red curve shown in figure 3, comparable to the data for the CORC<sup>®</sup>

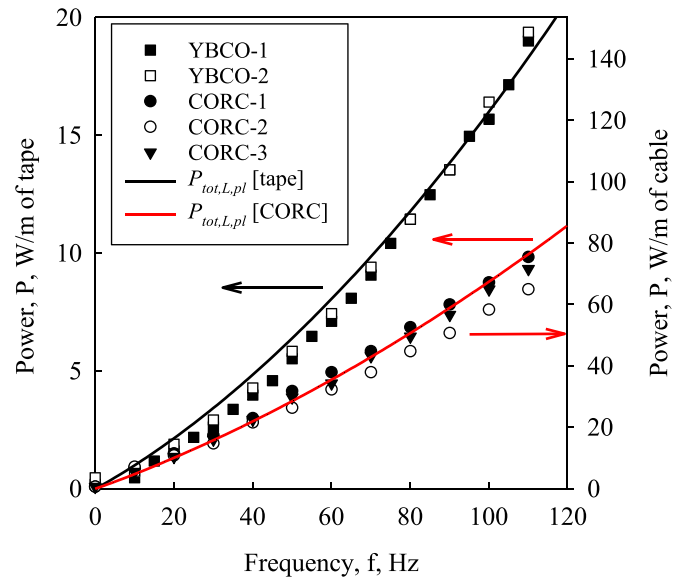


**Figure 3.** CORC<sup>®</sup> cable loss per meter of tape (left axis) and per meter or cable (right axis). Three measurement sets on the same cable, along with tape loss data (per meter of tape, left axis only) from figure 2. Both samples were oriented horizontally. The black line is the calculation for ReBCO tape with  $I_c = 35$  A, including the hysteretic loss (critical state), flux creep modification ( $n = 35$ ), and an eddy current loss component for a Cu strip  $80 \mu\text{m}$  thick with a  $RR = 3.8$  at  $77$  K [4]. The red solid line is similar calculation, with hysteretic (and flux creep) loss of tape multiplied by a factor of  $\pi/2$ , and eddy current loss multiplied by a factor of  $(\pi/2)^2$ , as described in text.

cable. The agreement is again reasonable. However, this leads to the immediate conclusion that the eddy current contribution in the cable is essentially the same as that in the tape, and that no tape-to-tape coupling currents appear to be present (i.e. the coupling currents are sufficiently small to lead to a negligible loss contribution for these particular samples). Of such cable level coupling currents were present, it would lead to a loss term which was proportional to  $f^2$  and inversely proportional to the tape-to-tape contact resistance. Evidently, the tape-to-tape contact resistance is sufficiently high that any cable level currents are negligible. This is consistent with numerous studies of tape-tape resistance in YBCO stack Interstrand Contact Resistance (ICR) measurements [45–49], as well as tape to tape resistance in Roebel cables [12], and CORC cables [17]. This is not surprising given that the cables were measured ‘as-received’. The observance of coupling currents is well known to hinge on the contact resistance between the tapes in Low Temperature Superconductor (LTSC) cables [50] as well as HTS cables [17]. We and many others have measured contact resistance between Cu surfaces, and these are well known to be controlled by the oxide layers which form on the Cu, whether the Cu is the Cu sheath of a low temperature superconductor (LTS) wire or the electroplated surface of a ReBCO tape. Of course, oils and other contaminants may further increase contact resistance, and alternatively, sintering, soldering, plating with other metals, or surface abrasion can reduce this value. Previous measurements on Roebel cables [51] and CORC cables in as received conditions from

our group have failed to show the signature of cable level coupling currents between the tapes in the respective cables. Of course, such currents can certainly be present in cables which have low values of interstrand contact resistance. An excellent recent paper which includes data on the AC loss of CORC cables at 77 K and 4 K shows this very clearly. Yagotintsev [17] shows loss as a function of frequency for a CORC cables in perpendicular applied fields at 77 K, with those with Sn soldering between the tapes showing two orders of magnitude lower contact resistance between tapes and an obvious coupling loss contribution, while the frequency response for the un-soldered is much lower (see figure 13 of Yagotintsev [17], that text). The relative contributions of strand level eddy currents and conductor power law properties are not discussed in this case. But, the overall message is similar, cables in ‘as-received’ states appear to have low coupling loss. However, as noted above these interstrand contact resistance values are highly sample preparation dependent. It is also important to distinguish between cable level, tape-to-tape coupling currents, and coupling currents between filaments formed by striation or other means within the tapes [7], where strand level coupling currents are readily seen.

In the case of the Roebel cable, a 10 cm segment of the cable was mounted horizontally, and the results are shown in figure 4. If we want an average  $I_c$  of the whole of the  $M$ – $H$  loop, we can use equation (1) to extract  $I_c$ , from the linear portion (green dashed line), obtaining a value of 60 A. This is reasonable since we have measured over a field range from 0 to 0.566 T, and thus can be expected to be somewhat lower than the nominal 100 A (77 K, self-field)  $I_c$  of the starting tape (a different tape than that used for the CORC<sup>®</sup> cable). We can also observe an upward curvature (as was seen for the tape and the CORC<sup>®</sup> cable), again indicating the presence of eddy currents for the Roebel cable. Given the relatively high contact resistances already measured for this cable under these preparation conditions [10], no coupling currents should be seen. The total loss calculation for hysteretic, flux creep modifications and eddy currents is shown as the black full line in figure 4, an  $I_c = 50$  A (reduced from the 50 estimated from the CSM, because of creep effects),  $n = 35$ , a Cu thickness of 30  $\mu\text{m}$  and a RR (77 K) = 3.5 was used. We thus infer that again no cable level currents are present, since the physically reasonable (for electroplated Cu), but the relatively low RR would be unphysically low if we attributed any of the eddy current losses to the cable level.

This paper has focused on losses in coated conductor cables under conditions of fast ramping applied external fields. If we think about the implications of the measurements and models above, we do see that relatively simple models for the loss of single tapes can be modified to predict the loss of cables wound from them, at least in the case where tape-to-tape coupling currents are not present, core losses (the CORC core) are not strong, and we are below the relevant skin depth frequencies. While we might have suspected that the models used at lower frequencies or field amplitudes could be applied at higher excitations, it was important to demonstrate this. Of course, coupling loss, core loss, and even skin depth modifications can be added to the analysis, when needed. We can apply

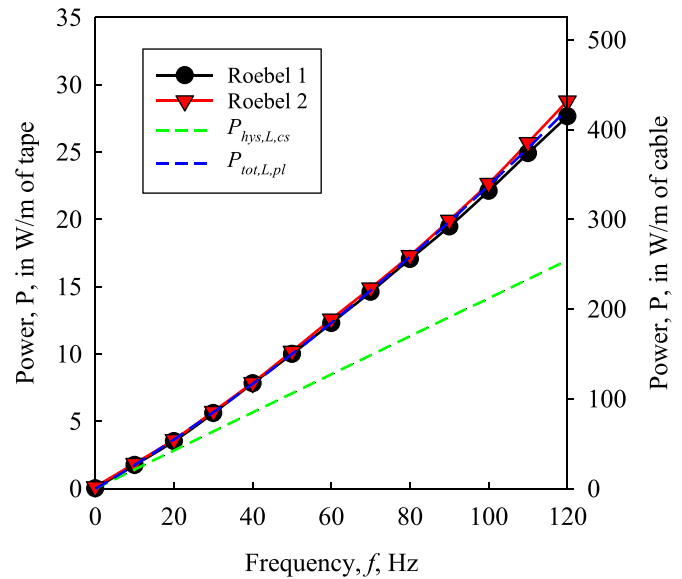


**Figure 4.** Roebel cable loss per meter of tape (left axis) and per meter of cable (right axis). Two measurements of the same cable are shown.  $I_c$  extracted from the loss expression is 50 A. The green dashed line is critical state hysteretic component, the red dashed line includes the critical hysteretic loss with creep modification ( $n = 35$ ), and an eddy current component with Cu layer thickness 30  $\mu\text{m}$  and RR (77 K) = 3.5.

equations (8) and (9) (tapes and Roebel cables) and equation (10) (CORC cables) to higher field amplitudes as long as the  $J_c$  we use is an average over the fields of the magnetic sweep. Similarly, we can apply the expressions in a straightforward manner to operation at different temperatures, assuming the  $J_c$  (as well as the stabilizer resistivity) is averaged over the field cycle at that temperature. One further important result is that at these higher values of  $dB/dt$ , it is important to include flux creep (or power law) effects in the analysis.

### 3. Conclusions

We have measured ReBCO coated conductor based CORC<sup>®</sup> and Roebel cables at 77 K in an SMC that subjected the tapes in the sample to a radial field of 566 mT at frequencies up to 120 Hz with an approximately sinusoidal waveform. This leads to average (over the cycle) ramp rate of 272 T s<sup>-1</sup>. The samples were oriented such that the field applied to the tapes within the cables were only radial, simplifying the analysis. An expression for loss for which includes hysteretic, flux creep, and eddy current losses is fit to both the CORC<sup>®</sup> and the Roebel cables. This expression allows easy comparison of the relative influence of eddy currents and flux creep (or power-law behavior) effects. The losses of the Roebel cable are approximately consistent with those of a tape of the given filament width. The losses of the CORC<sup>®</sup> cable were seen to be lower than those of the tapes it is wound with due to the helical twist of the tapes. Once correcting the hysteretic and eddy current components by the geometrical correction factors  $(2/\pi)$  and  $(2/\pi)^2$ , respectively, the CORC<sup>®</sup> agrees well with the model.



Hysteretic losses, as expected, dominated the loss. Assuming an  $n = 35$ , we found flux creep effects to add  $\cong 26\%$  at 100 Hz as compared to the critical state hysteretic loss, and eddy currents to be about equal to the hysteretic loss (at 120 Hz) for the CORC<sup>®</sup> cable. Finally, we find that both the loss of the CORC<sup>®</sup> and Roebel measured here are essentially the sum of the hysteretic loss, flux creep effects, and normal metal eddy current losses of the individual tapes. The losses of these cables have been measured at quite high  $B \times dB/dt$  with no coupling current loss observed under the present preparation conditions (although lower inter-tape contact values would no doubt lead to these). One further important result is that at these higher values of  $dB/dt$ , it is important to include flux creep (or power law) effects in the analysis. These measurement and models in this work should prove useful for designs of superconducting machinery or applications where coated conductor cables are used in fast ramping external fields.

### Data availability statement

The data that support the findings of this study are available upon reasonable request from the authors.

### Acknowledgments

This work was supported by the Air Force Office of Scientific Research (AFOSR) under effort LRIR #14RQ08COR, the Aerospace Systems Directorate at Air Force Research Laboratory (AFRL), the U.S. Air Force Summer Faculty Fellowship Program (AFSFFP), and the U.S. Department of Energy, Office of Science and Office of High Energy Physics, under Award Number DE SC0011721.

### ORCID iDs

M D Sumption  <https://orcid.org/0000-0002-4243-8380>  
D C van der Laan  <https://orcid.org/0000-0001-5889-3751>

### References

- [1] Haran K *et al* 2017 High power density superconducting rotating machines—development status and technology roadmap *Supercond. Sci. Technol.* **30** 123002
- [2] van der Laan D C 2009 *Supercond. Sci. Technol.* **22** 065013
- [3] van der Laan D C, Weiss J D and McRae D M 2019 Status of CORC<sup>®</sup> cables and wires for use in high-field magnets and power systems a decade after their introduction *Supercond. Sci. Technol.* **32** 033001
- [4] Long N J, Badcock R A, Hamilton K, Wright A, Jiang Z and Lakshmi L S 2010 Development of YBCO Roebel cables for high current transport and low AC loss applications *J. Phys.: Conf. Ser.* **24** 022021
- [5] Majoros M, Sumption M D, Collings E W and van der Laan D C 2014 *Supercond. Sci. Technol.* **27** 125008
- [6] Gömöry F, Šouc J, Vojenčiak M and Solovyov M 2015 *IEEE Trans. Appl. Supercond.* **25** 8201004
- [7] Vojenčiak M, Kario A, Ringsdorf B, Nast R, van der Laan D C, Scheiter J, Jung A, Runtsch B, Gömöry F and Goldacker W 2015 *Supercond. Sci. Technol.* **28** 104006
- [8] Terzioğlu R, Vojenčiak M, Sheng J, Gömöry F, Çavuş T F and Belenli İ 2017 *Supercond. Sci. Technol.* **30** 085012
- [9] Šouc J, Gömöry F, Kóvač J, Nast R, Jung A, Vojenčiak M, Grilli F and Goldacker W 2013 *Supercond. Sci. Technol.* **26** 075020
- [10] Lakshmi L S, Thakur K P, Staines M P, Badcock R A and Long N J 2009 *IEEE Trans. Appl. Supercond.* **19** 3361
- [11] Lakshmi L S, Long N J, Badcock R A, Staines M P, Jiang Z, Thakur K P and Emhofer J 2011 *IEEE Trans. Appl. Supercond.* **21** 3311
- [12] Majoros M, Sumption M D, Collings E W and Long N J 2014 Stability, inter-strand contact resistance, and AC losses in YBCO Roebel cables *IEEE Trans. Appl. Supercond.* **24** 6600505
- [13] Yang Y *et al* 2016 *IEEE Trans. Appl. Supercond.* **26** 8202105
- [14] Schuller S, Goldacker W, Kling A, Krempasky L and Schmidt C 2007 *Physica C* **463–465** 761–5
- [15] Terzieva S, Vojenčiak M, Pardo E, Grilli F, Drechsler A, Kling A, Kudymow A, Gömöry F and Goldacker W 2010 *Supercond. Sci. Technol.* **23** 014023
- [16] Kovacs C, Majoros M, Sumption M D and Collings E W 2019 Magnetization measurements of CORC<sup>®</sup> and Roebel type YBCO cables for accelerators using a  $\pm 3$ -T dipole magnetometer *IEEE Trans. Appl. Supercond.* **29** 8200905
- [17] Yagotintsev K, Anvar V A, Gao P, Dhalle M J, Haugan T J, van der Laan D C, Weiss J D, Hossain M S A and Nijhuis A 2020 AC loss and contact resistance in REBCO CORC<sup>®</sup>, Roebel, and stacked tape cables *Supercond. Sci. Technol.* **33** 085009
- [18] Solovyov M, Šouc J and Gömöry F 2014 AC loss properties of single-layer CORC cables *J. Phys.: Conf. Ser.* **507** 022034
- [19] Goo J, Han J W, Lee S, Kim W S, Choi K and Lee J K 2021 Magnetization loss of CORC with various configurations of 2G HTS strands *IEEE Trans. Appl. Supercond.* **31** 5901205
- [20] Tian M, Yang J, Shen B, Öztürk Y, Ma J, Li C, Shah A, Patel I, Li J and Coombs T 2021 Magnetization loss characteristics in superconducting conductor on round core cables with a copper former *IEEE Trans. Appl. Supercond.* **31** 4803204
- [21] Li W, Sheng J, Zheng J, Wu Y, Guo C, Li Z and Jin Z 2021 Study on reducing magnetization loss in CORC cables by laser cutting technology *IEEE Trans. Appl. Supercond.* **31** 4802009
- [22] Demencik E, Grilli F, Kario A, Nast R, Jung A, Vojenčiak M, Scheiter J and Goldacker W 2015 AC magnetization loss and transverse resistivity of striated YBCO coated conductors *IEEE Trans. Appl. Supercond.* **25** 8201405
- [23] Wang Y, Wang Y, Wei D, Guo T, Meng Y, Wang J and Kan C 2020 AC losses of a CORC-like conductor using accelerated 3D T-A model *Physica C* **579** 1353770
- [24] van Nugteren J *et al* 2016 Measurement and numerical evaluation of AC losses in a ReBCO Roebel cable at 4.5 K *IEEE Trans. Appl. Supercond.* **26** 8201407
- [25] Pardo E, Kapolka M, Kovác J, Šouc J, Grilli F and Piqué A 2016 Three-dimensional modeling and measurement of coupling AC loss in soldered tapes and striated coated conductors *IEEE Trans. Appl. Supercond.* **26** 4200607
- [26] Gao P *et al* 2019 Inter-strand resistance and AC loss in resin-filler impregnated ReBCO Roebel cables *Supercond. Sci. Technol.* **32** 125002
- [27] Yan Y, Qu T and Grilli F 2021 Numerical modeling of AC loss in HTS coated conductors and Roebel cable using T-A formulation and comparison with H formulation *IEEE Access* **9** 49649
- [28] Murphy J P, Gheorghiu N N, Haugan T, Sumption M D, Majoros M and Collings E W 2017 *Cryogenics* **86** 57–69
- [29] Brandt E H and Indenbom M 1993 *Phys. Rev. B* **48** 12893

- [30] Brandt E H 1994 *Phys. Rev. B* **49** 9024
- [31] Muller K-H 1997 *Physica C* **281** 1–10
- [32] Sumption M D, Lee E, Cobb C B, Barnes P N, Haugan T J, Tolliver J, Oberly C E and Collings E W 2003 *IEEE Trans. Appl. Supercond.* **13** 3553
- [33] Sumption M D, Barnes P N and Collings E W 2005 *IEEE Trans. Appl. Supercond.* **15** 2815
- [34] Carr W J 2001 *AC Loss and Macroscopic Theory of Superconductors* 2nd edn (London: Taylor and Francis)
- [35] Grilli F, Pardo E, Stenvall A, Nguyen D N, Yuan W and Gömöry F 2014 Computation of losses in HTS under the action of varying magnetic fields and currents *IEEE Trans. Appl. Supercond.* **24** 8200433
- [36] Kapolka M, Zermeno V M R, Zou S, Morandi A, Ribani P L, Pardo M E and Grilli F 2018 Three-dimensional modeling of the magnetization of superconducting rectangular-based bulks and tape stacks *IEEE Trans. Appl. Supercond.* **28** 8201206
- [37] Pust L 1990 Comparison between conventional flux creep in constant magnetic field and the effect of creep on the shape of magnetic hysteresis loops in high  $T_c$  superconductors *Supercond. Sci. Technol.* **3** 598–601
- [38] Thakur K P, Raj A, Brandt E H and Sastry P 2011 Frequency dependent magnetization of superconductor strip *Supercond. Sci. Technol.* **24** 045006
- [39] Brandt E H 1997 Susceptibility of superconductor disks and rings with and without flux creep *Phys. Rev. B* **55** 14514
- [40] Jonsson B J, Rao K V, Yun S H and Karlsson U O 1998 Method to extract the critical current density and the flux-creep exponent in high- $T_c$  thin films using ac susceptibility measurements *Phys. Rev. B* **58** 5862
- [41] Chen D-X and Pardo E 2006 Power-law E (J) characteristic converted from field-amplitude and frequency dependent ac susceptibility in superconductors *Appl. Phys. Lett.* **88** 222505
- [42] Mawatari Y 1996 *Phys. Rev. B* **54** 13215
- [43] Brandt E H 1996 *Czechoslovak J. Phys.* **46** 893
- [44] Okii Y, Taguchi J, Takahashi H, Yasutake H, Kako E, Michizono S and Yamamoto Y 2019 R&D of copper electroplating process for power couplers: effect of microstructure on RRR *19th Int. Conf. on RF Superconductivity* (<https://doi.org/10.18429/JACow-SRF2019-M0P083>)
- [45] Xue S, Sumption M D and Collings E W 2021 YBCO coated conductor interlayer electrical contact resistance measured from 77 K to 4 K under applied pressures up to 9.4 MPa *IEEE Trans. Appl. Supercond.* **31** 7000305
- [46] Kovacs C J, Sumption M D, Majoros M and Collings E W 2020 Modified interconductor contact resistivity in coated conductor stacks and Roebel cables *IEEE Trans. Appl. Supercond.* **30** 6600505
- [47] Bonura M, Barth C, Joudrier A, Troitino J F, Fête A and Senatore C 2019 Systematic study of the contact resistance between REBCO tapes: pressure dependence in the case of no-insulation, metal co-winding and metal-insulation *IEEE Trans. Appl. Supercond.* **29** 6600305
- [48] Lu J, Goddard R, Han K and Hahn S 2017 Contact resistance between two REBCO tapes under load and load cycles *Supercond. Sci. Technol.* **30** 045005
- [49] Lu J, Levitan J, McRae D and Walsh R 2018 Contact resistance between two REBCO tapes: the effects of cyclic loading and surface coating *Supercond. Sci. Technol.* **31** 085006
- [50] Sumption M D, Collings E W, Scanlan R M, Nijhuis A, Ten Kate H H J, Kim S W, Wake M and Shintomi T 1999 Influence of strand surface condition on interstrand contact resistance and coupling loss in NbTi-wound Rutherford cables *Cryogenics* **39** 197–208
- [51] Lakshmi L S, Staines M P, Badcock R A, Long N J, Majoros M, Collings E W and Sumption M D 2010 Frequency dependence of magnetic ac loss in a Roebel cable made of YBCO on a Ni–W substrate *Supercond. Sci. Technol.* **23** 085009